# DESIGN AND SIMULATION OF THREE-DEGREE-OF-FREEDOM WRIST STRUCTURE OF PICKING MANIPULATOR
/
# 采摘机械手三自由度腕部结构设计及仿真

**Junhui SUN [1)], Jinliang GONG [2*)], Yanfei ZHANG [1*)]**
[1)]School of Agricultural Engineering and Food Science, Shandong University of Technology, Zibo/China
[2)]School of Mechanical Engineering, Shandong University of Technology, Zibo/China
*Tel: +8618265338441; E-mail: 1392076@sina.com; gjlwing@sdut.edu.cn*
*DOI: https://doi.org/10.35633/inmateh-71-66*

***Keywords**: underactuated, picking manipulator, cardan joint, optimised design, ANSYS*

## ABSTRACT
*In order to solve the problem of poor flexibility of existing picking manipulators, a picking manipulator with a wrist joint has been designed, the wrist is capable of rotating 45° forward and backward around the x and y axes. Firstly, ANSYS was used to simulate the performance of different hoses under different conditions, and finally a 4*6mm PVC hose was selected to replace the internal cardan joint as the transmission component. Secondly, the wrist structure was optimized using genetic algorithm to reduce the tendon rope variation differences to 0.31mm and 0.24mm. Finally, the results of orchard picking experiments indicate that the end-effector rotation of 720° can ensure that the fruit stalks can be unscrewed, the time required to complete the picking is 1.6s, and the overall picking success rate was 100%. After 9 days of placing the harvested fruit, both the flesh and skin are intact, indicating that the manipulators can complete the non-destructive picking operation.*

## 摘要
*为了解决现有采摘机械手灵活性差的问题，设计了一种带有腕部关节的采摘机械手，其腕关节可绕 x 轴和 y 轴正负旋转 45°。首先，使用 ANSYS 对不同软管在不同工况下的性能进行了仿真，最终选择了 4*6mm 的 PVC 软管代替内部万向节作为传动部件。其次，利用遗传算法对腕部结构进行优化，将腱绳的变化量差值缩小到 0.31mm 和 0.24mm。最后，果园采摘实验结果表明，末端执行器旋转 720°可确保拧断果柄，完成采摘所需的时间为 1.6 秒，整体采摘成功率为 100%。采摘的果实放置 9 天后，果肉和果皮都完好无损，表明机械手可以完成无损采摘操作。*

## INTRODUCTION
At present, the harvesting operation of fruit and vegetable products has the characteristics of concentrated cycle, large amount of labour and mainly manual operation *(Bao et al., 2013 )*, The reduction of labour, the cost of labour increases to promote the development of mechanized harvesting *(Bu et al., 2020)*, the expansion of the scale of the standardized orchard, for the orchard intelligent, mechanization provides favourable conditions *(Li et al., 2021)*.and efficient picking robots can help to realize the automation of picking operation *(Chen et al., 2023)*, in which the picking manipulator as an actuator, and its performance determines the efficiency and quality of the picking operation.

*Chen et al., (2021),* designed a fully pneumatic suction-clamp integrated tomato picking end-effector, which completes the picking operation in four steps: adsorption, pull-back, clamping, and twisting. *Yu et al., (2022),* developed a tomato picking robot with autonomous recognition capability and soft three-finger gripping jaws capable of non-destructive picking. To evaluate the performance of end effectors used in soft tree fruit harvesting, *Goulart et al., (2023),* has defined a set of measurement standards. *Stevanović et al., (2023)*, designed a composite 6-DOF robot harvester with telescopic robot arm for plum farmyards, it can carry the picked fruits to the designated location. *Vítor et al., (2023)*, proposed a stackable 3 DoF SCARA manipulator for tomato harvesting. the manipulator was able to position itself very close to the target in less than 3 seconds, where an end-effector could adjust its position for the picking. *Boisclair et al., (2022)* designed a hand with 17 degrees of freedom with a manually operable thumb structure that allows the hand to have three different grasping postures.

[1] *Junhui SUN, M.S. Eng.; Jinliang GONG, A. Prof. Ph.D. Eng.; Yanfei ZHANG, Prof. Ph.D. Eng.*

*Hohimer et al., (2019)* and *Hua et al., (2023)* design of pneumatic flexible picking hand claw has little damage to the surface of fruits and vegetables. Flexible end-effector enables non-destructive picking operations, as shown by pulp damage studies conducted by *Bu et al., (2020)*. Pneumatic finger gripping is faster and has better adaptability compared to tendon-driven ones.

Various scholars have achieved remarkable results in the field of picking robots, but the current picking robots still have the following problems. The manipulator usually uses pulling *(Zhi et al., 2023)*, twisting, and cutting of fruit stalks to carry out picking operations. The picking method of pulling off the fruit stalk is relatively simple *(Wang et al., 2023)*, but it requires the robotic arm to provide a large pulling force as well as displacement, and it is also prone to cause the branch to sway, resulting in the dislodging of other fruits. The drive and end-effector of the picking manipulators designed in *Long et al., (2023)* and *Zhang et al., (2023)* cannot be separated, resulting in large size and weight. If the picking method of unscrewing the fruit stalk is used, the end-effector and driver need to be rotated together, which reduces the flexibility, and the picking space is narrow, and the large size is not conducive for the robotic arm to adjust the position of the end-effector.

In order to solve the problem of poor flexibility of the existing manipulator, this paper designs a rope-driven underactuated apple picking manipulator with three rotational degrees of freedom wrist joints based on the double cardan joint structure, which has higher flexibility, versatility, and can realise high-efficiency and non-destructive picking.

## MATERIALS AND METHODS

### *Manipulator configuration analysis and design*

Compared with fully actuated end-effector, underactuated end-effector has the advantages of simple structure and small size. At the same time, the adaptability of underactuated end-effector is more suitable for gripping objects of different shapes and sizes *(Wei et al., 2021)*. The rope-driven type has a simple structure and smaller size, and it meets the gripping force requirements of fruit and vegetable picking although the gripping force of the end-effector is smaller.

When the length of the finger is certain, the higher the number of knuckles, the better the envelope of the finger to a round object, but the stable grasping space of the finger will decrease, resulting in an increase in the force required for stable grasping. In contrast, a finger with 3 knuckle units has better envelopment and a larger stable grasping space. The gripping object of the manipulator is a spherical fruit, and 3 fingers can complete the gripping. Therefore, the end-effector selection of 3 circumferential uniform distribution of the fingers, the number of knuckles of each finger is 3.

There are three main ways for picking robots to pick apples: cutting, pulling and twisting the stalk. The direct pulling of apples by the robot will cause the branch to shake, which will result in branch damage and the shedding of the rest of the ripe fruits, and the pulling process requires a larger pulling force and stroke. If a blade is used to cut the stalk for picking, a force of 18-28 N is required to cut the stalk (Table 1), compared to the much less vigorous method of twisting the stalk, which requires only 2-5 N (Table 2) *(Deng et al., 2019)*.

**Table 1**

**Apple stalk cutting force**

| Diameter/mm | 58.33 | 64.2 | 72.5 | 82.1 | 90.5 |
|---|---|---|---|---|---|
| Cutting force/N | 18.2 | 21.3 | 23.3 | 25.2 | 27.8 |

**Table 2**

**Apple stalk twisting force**

| Diameter /mm | 62.1 | 71.6 | 77.8 | 83.5 | 88.4 | 91.3 |
|---|---|---|---|---|---|---|
| Twisting force/N | 2.34 | 3.24 | 3.55 | 3.86 | 3.99 | 4.21 |

Combining the above analyses, a rope-driven underactuated apple picking manipulator with rotary unscrewing of the fruit stalk as the picking method and a wrist structure with three rotational degrees of freedom was designed, as shown in Fig. 1.

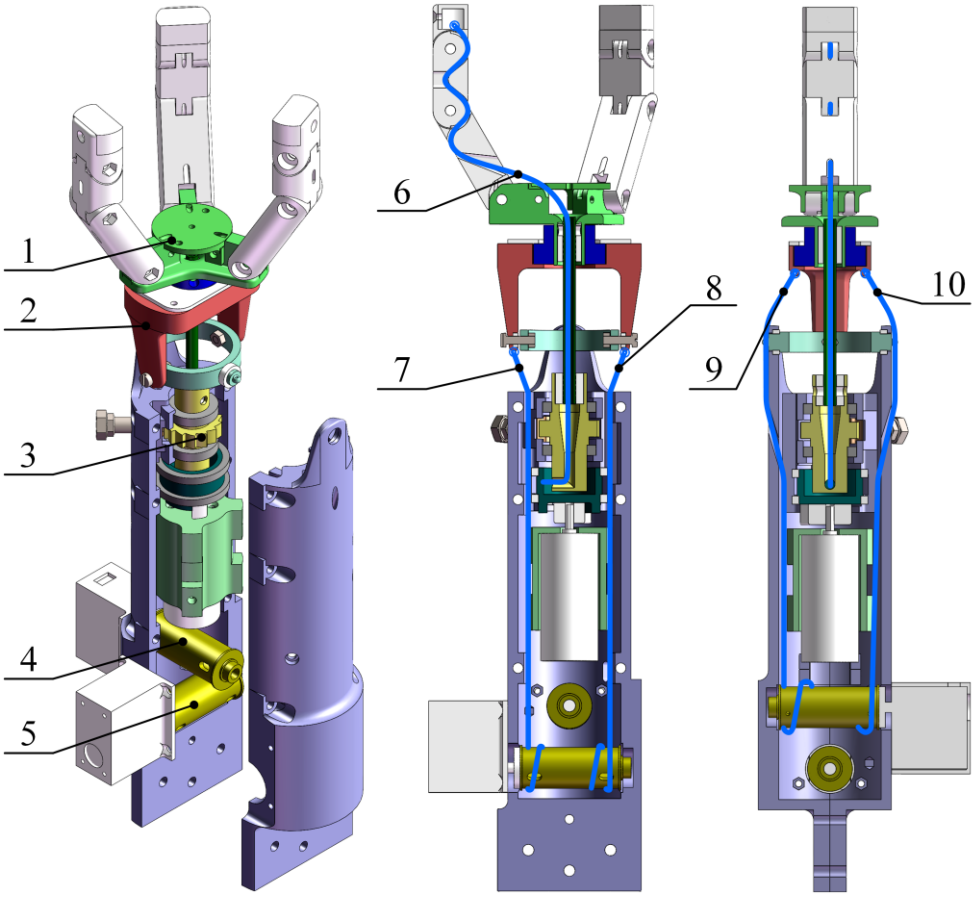


**Fig. 1 – Rope-driven underactuatedn picking manipulator**

*1. End-effector; 2. Wrist module; 3. End-effector drive module; 4. Winding spool I; 5. Winding spool II; 6. Tendon rope I; 7. Tendon rope II; 8. Tendon rope III; 9. Tendon rope IV; 10. Tendon rope V*

The manipulator includes an underdriven end-effector, a three rotational degrees of freedom wrist module and a drive module. The three fingers in the end-effector are uniformly distributed around the circumference, and are driven by a tendon rope to close it and torsion springs at the knuckle to open it. And the three fingers are ultimately driven by a tendon rope, so that the movement of the three fingers is synchronized. The end-effector drive module is responsible for controlling the opening and closing as well as the rotation of the end-effector. The wrist module can rotate 45° clockwise and counterclockwise around the *x* and *y* axes, and adopts a double cardan joint type structure with inner and outer nesting, as shown in Fig. 2., so that the end-effector can rotate continuously in a full circle while the wrist is deflected.

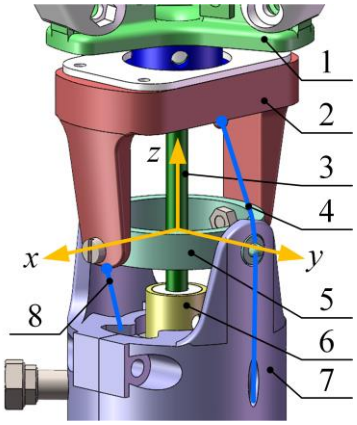


**Fig. 2 – Three rotational degrees of freedom wrist structure**

*1. end-effector; 2. n-bracket; 3. Hose; 4. tendon rope V; 5. circular bracket; 6. output shaft; 7. Shell; 8. tendon rope II*

The tendon rope II and III in the opposite direction wrapped in the winding spool II, the winding spool II rotation can make a tendon rope downward tightening at the same time upward relaxation of the other tendon rope, so as to drive the wrist around the y-axis rotation. When the wrist rotates around the y-axis, in order to avoid non-essential rotation of the wrist around the x-axis due to changes in the tension of the tendon cords

IV and V, it is necessary to ensure that the tendon cords IV and V pass through a point on the y-axis. So that the wrist around the y-axis rotation, tendon rope IV, V is always in a taut state.

Since the underdriven end-effector is remotely driven by a tendon rope, in order to avoid entanglement of the tendon rope I driving the end-effector with the output shaft during the end-effector rotation, it is necessary to ensure that the tendon rope I passes through the centre of the cardan joints, however, the existing standard parts of the cardan joints cannot satisfy this requirement. Moreover, when installing the inner and outer nested double cardan joint structure, it is necessary to ensure that the centres of the two cardan joints coincide, which requires high installation accuracy. In order to reduce the installation difficulty and the manufacturing cost of non-standard parts, a hose is used instead of the internal cardan joint as the transmission component.

***Hose Simulation and Selection***

The main function of the hose is to transmit the torque from the output shaft to drive the end-effector to rotate. There are three kinds of working conditions: transmitting torque in the vertical state, bending, and transmitting torque in the bending state. Using ANSYS to simulate three working conditions, and based on the simulation results, with the premise of meeting the harvesting requirements and the goal of excellent transmission efficiency, the selection of hoses is carried out.

In order to reduce the manufacturing cost of non-standard parts, the hose selects the common ones on the market, naming the different materials and specifications, see Table 3, and the properties of different materials are shown in Table 4.

**Table 3**

**Hose Nomenclature**

| Inner Diameter*Outer Diameter (mm) | 3*5 | 4*6 | 4*8 | 6*8 | 6*10 | 8*10 | 8*12 |
|---|---|---|---|---|---|---|---|
| Silicone Hose | G-1 | G-2 | G-3 | G-4 | G-5 | G-6 | G-7 |
| Rubber Hose | X-1 | X-2 | X-3 | X-4 | X-5 | X-6 | X-7 |
| PVC Hose | P-1 | P-2 | P-3 | P-4 | P-5 | P-6 | P-7 |
| TPU Hose | T-1 | T-2 | T-3 | T-4 | T-5 | T-6 | T-7 |

**Table 4**

**Table of material properties**

| Name | Young's modulus (GPa) | Densities (kg/m$^3$) | Poisson's ratio |
|---|---|---|---|
| Silicone Hose | 0.12 | 1120 | 0.48 |
| Rubber Hose | 0.83 | 1343 | 0.45 |
| PVC Hose | 0.47 | 1020 | 0.41 |
| TPU Hose | 1.62 | 950 | 0.42 |

According to Table 2, it can be seen that the maximum torque required to unscrew the fruit stalk is about 0.2 N•mm. Considering the obstruction of branches during the rotation process, the load during the hose rotation process is set to 0.6 N•mm. When the wrist is in a vertical state, fix the revolute II and III, and apply a clockwise torque of 0.6 N•mm at the palm to simulate the deformation of the hose, which is the rotation angle $S$ of the palm, as shown in Fig.3(a).

The torque $N_1$ required for bending the hose was simulated by rotating the $n$-bracket 45° clockwise with the revolute I and III fixed, as shown in Fig. 3(b).

After the n-type bracket is rotated 45° around the x-axis, the output shaft is made to rotate at a speed of 1 r/min at a constant speed for the whole circumference, and the required torque $N_2$ of the output shaft is simulated, as shown in Fig. 3(c).

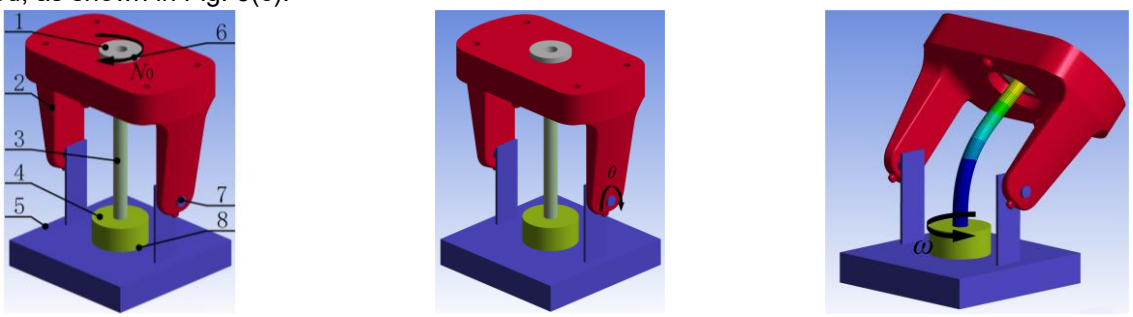


(a) Torsion simulation in wrist vertical state (b) Wrist rotation simulation (c) Torsion simulation in wrist deflection state

**Fig. 3 – Hose simulation under different working conditions**

*1. palm; 2. n-bracket; 3. Hose; 4. output shaf;t 5. Shell; 6. revolute I; 7. revolute II; 8. revolute III*

Build an evaluation function as:

$$p = S + N_1 + N_2 \quad (1)$$

where: $p$ is value of evaluation; $S$ is rotation angle of the palm, [°]; $N_1$ is torque required for bending the hose, [N•mm]; $N_2$ is required torque of the output shaft, [N•mm].

The smaller value $p$ of the evaluation function represents the higher transmission efficiency of the hose. The simulation results are shown in Table 5, The simulation results are shown in Table 5, G-1, G-2, G-4 and G-6 undergo large deformation during the simulation and cannot meet the design requirements. The hose with an inner diameter of 4mm, an outer diameter of 6mm and a material of PVC is finally selected.

**Table 5**

**Hose simulation results**

| Name | $S$ (°) | $N_1$ (N•mm) | $N_2$ (N•mm) | $p$ | Name | $S$ (°) | $N_1$(N•mm) | $N_2$(N•mm) | $p$ |
|---|---|---|---|---|---|---|---|---|---|
| P-1 | 273.75 | 87.07 | 106.52 | 467.34 | T-1 | 65.18 | 297.21 | 386.76 | 749.15 |
| P-2 | 113.32 | 157.30 | 186.42 | 457.04 | T-2 | 34.67 | 537.81 | 781.36 | 1353.84 |
| P-3 | 31.39 | 597.77 | 684.73 | 1313.89 | T-3 | 9.49 | 1325.43 | 1867.32 | 3202.24 |
| P-4 | 42.54 | 290.76 | 342.16 | 675.46 | T-4 | 12.84 | 904.03 | 1367.35 | 2284.22 |
| P-5 | 13.85 | 1181.17 | 1422.30 | 2617.32 | T-5 | 4.17 | 2063.98 | 2864.80 | 4932.95 |
| P-6 | 20.18 | 659.99 | 936.27 | 1616.43 | T-6 | 6.09 | 1569.40 | 2606.80 | 4182.29 |
| P-7 | 7.25 | 1430.86 | 1923.60 | 3361.70 | T-7 | 1.45 | 2965.34 | 4125.20 | 7091.99 |
| G-1 | 314.08 | 22.34 | Invalid | | X-1 | 119.23 | 117.65 | 245.36 | 482.24 |
| G-2 | 268.28 | 40.51 | Invalid | | X-2 | 64.93 | 194.46 | 398.62 | 658.01 |
| G-3 | 127.38 | 152.54 | 209.38 | 498.30 | X-3 | 17.85 | 732.61 | 1263.50 | 2013.96 |
| G-4 | 155.57 | Invalid | | | X-4 | 24.16 | 359.35 | 668.23 | 1051.74 |
| G-5 | 56.17 | 306.10 | 389.46 | 751.73 | X-5 | 7.86 | 1460.10 | 2036.50 | 3504.46 |
| G-6 | 87.00 | Invalid | | | X-6 | 11.46 | 445.85 | 1564.23 | 2021.54 |
| G-7 | 29.40 | 403.30 | 559.78 | 992.48 | X-7 | 2.74 | 2049.00 | 3698.24 | 5749.98 |

***Optimization of wrist structure and building control models***

The structural schematic diagram of the wrist rotating around the y-axis is shown in Fig. 4, and a polar coordinate system is established with the centre of rotation H of the circular bracket as the pole and the counterclockwise direction as the positive direction. In the figure, point I ($l_{HI}$,-$\eta$) is the contact point between the tendon rope and the shell, and point J ($l_{HJ}$,0) is the fixation point of the tendon rope on the circular bracket.

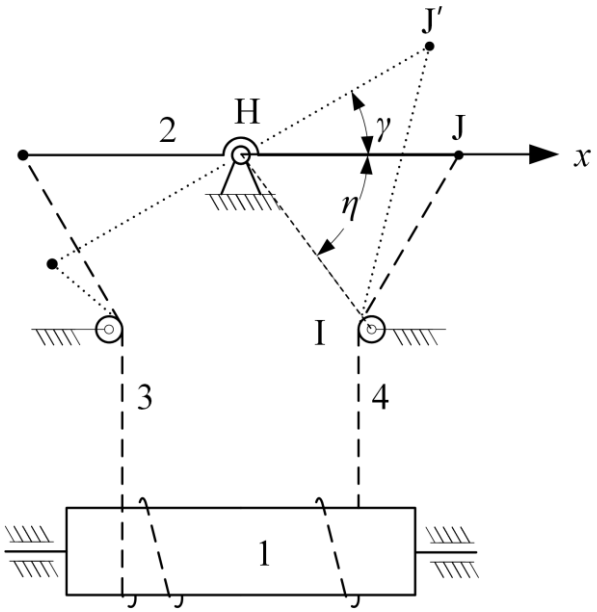


**Fig. 4 – Wrist rotation around y-axis structure schematic diagram**

*1. winding spool II; 2. circular bracket; 3. tendon rope II; 4. tendon rope III*

When the circular bracket is rotated counterclockwise by an angle $\gamma$, the length change of tendon rope III and tendon rope II is:

$$\Delta l_3 = \left| \sqrt{l_{HI}^{\ 2} + l_{HJ}^{\ 2} - 2\cos(\eta+\gamma) l_{HJ} l_{HI}} - l_{JI} \right| \tag{2}$$

$$\Delta l_2 = \left| \sqrt{l_{HI}^{\ 2} + l_{HJ}^{\ 2} - 2\cos(\eta-\gamma) l_{HJ} l_{HI}} - l_{JI} \right| \tag{3}$$

in which,

$l_{JI} = \sqrt{l_{HI}^{\ 2} + l_{HJ}^{\ 2} - 2\cos\eta l_{HJ} l_{HI}}$; $l_{HI} = \frac{22.2}{\cos\eta}$; $l$ is the distance between two points, [mm]; $\gamma$ is angle of rotation of circular bracket, [°]; $\Delta l_3$ is length change of tendon rope III, [mm]; $\Delta l_2$ is length change of tendon rope II, [mm];

The difference in the length change of tendon ropes II and III is:

$$\Delta l_{23} = f(\gamma) = \left| \Delta l_2 - \Delta l_3 \right| \tag{4}$$

in which, $\Delta l_{23}$ is difference in the length change of tendon ropes II and III, [mm].

Combining Equation (2), (3) shows that the difference in the length change of tendon rope is affected by $\eta$, $\gamma$ and $l_{HJ}$.

$$\frac{df}{d\gamma} = \frac{\sin(\eta+\gamma) l_{HJ} l_{HI}}{\sqrt{l_{HI}^{\ 2} + l_{HJ}^{\ 2} - 2\cos(\eta+\gamma) l_{HJ} l_{HI}}} - \frac{\sin(\eta-\gamma) l_{HJ} l_{HI}}{\sqrt{l_{HI}^{\ 2} + l_{HJ}^{\ 2} - 2\cos(\eta-\gamma) l_{HJ} l_{HI}}} \tag{5}$$

Since Equation (5) is not constant to zero, the two tendon ropes do not change in length by the same amount during the rotation of the circular bracket.

The structural schematic diagram of the wrist rotation around the x-axis is shown in Fig. 5. A polar coordinate system is established with the *n*-bracket rotation centre K as the pole and the counterclockwise direction as the positive direction. The rotation process can be divided into two stages, the tendon rope and shell contact stage and separation stage. In the figure, the point N($l_{KN}$, $K$) is the contact point between the tendon rope and the shell, the point M($l_{KM}$, $\pi/2$) is the necessary point on the axis of the rotation axis of the *n*-bracket through which the tendon rope passes, and the point O($l_{KO}$, $\xi$) is the fixation point of the tendon rope on the circular bracket.

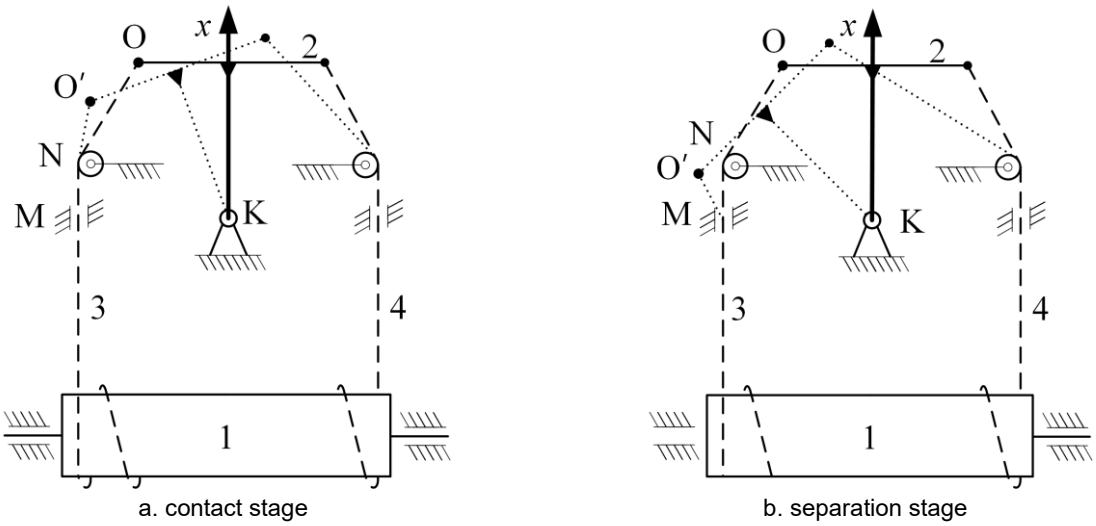


a. contact stage b. separation stage

**Fig. 5 – Wrist rotation around the *x*-axis structure schematic diagram**

*1. winding spool I; 2. n-bracket; 3. tendon rope IV; 4. tendon rope V*

Points O, N and M are collinear when the *n*-bracket is turned counterclockwise by an angle $\zeta_0$. The slopes of the line ON and the line NM are equal.

$$\frac{l_{KN}\sin\kappa - l_{KO}\sin(\xi+\zeta_0)}{l_{KN}\cos\kappa - l_{KO}\cos(\xi+\zeta_0)} = \frac{l_{KM} - l_{KN}\sin\kappa}{-l_{KN}\cos\kappa} \tag{6}$$

When the *n*-bracket is rotated counterclockwise by an angle $\zeta$, the change $\Delta l_4$ in the length of the tendon rope IV is:

$$\Delta l_4 = \begin{cases} \left| \sqrt{l_{KO}{}^2 + l_{KN}{}^2 - 2\cos(\kappa - \xi - \zeta) l_{KO} l_{KN}} - l_{ON} \right| & \zeta \le \zeta_0 \\ \left| \sqrt{l_{KO}{}^2 + l_{KM}{}^2 - 2\cos(\frac{\pi}{2} - \xi - \zeta) l_{KO} l_{KM}} - l_{ON} - l_{NM} \right| & \zeta > \zeta_0 \end{cases} \quad (7)$$

where,

$$\kappa = \frac{\pi}{2} - \arccos\frac{30}{l_{KN}};\ l_{MN} = \sqrt{l_{KM}{}^2 + l_{KN}{}^2 - 2\cos(\frac{\pi}{2} - \kappa) l_{KN} l_{KM}};\ l_{ON} = \sqrt{l_{KO}{}^2 + l_{KN}{}^2 - 2\cos(\kappa - \xi) l_{KN} l_{KO}};$$

$l$ is the distance between two points, [mm]; $\zeta$ is angle of rotation of *n*-bracket, [°]; $\Delta l_4$ is length change of tendon rope IV, [mm];

In order to make the change $\Delta l_4$ in the length of the tendon rope IV with the angle $\zeta$ of rotation similar in the two phases, let $l_{KN} = l_{KM}$.

The tendon rope V is always in contact with the shell and its length change $\Delta l_5$ is:

$$\Delta l_5 = \left| \sqrt{l_{KO}{}^2 + l_{KN}{}^2 - 2\cos(\kappa - \xi + \zeta) l_{KO} l_{KN}} - l_{ON} \right| \quad (8)$$

where, $\Delta l_5$ is length change of tendon rope V, [mm].

The difference $\Delta l_{45}$ in the amount of change in the length of tendon ropes IV and V is:

$$\Delta l_{45} = g(\zeta) = |\Delta l_4 - \Delta l_5| \quad (9)$$

In which, $\Delta l_{45}$ is difference in the length change of tendon ropes IV and V, [mm].

Combined with Equation (7)(8), known $l_{\mathrm{KM}}$ is 31, it can be seen that the difference in the length change of tendon ropes IV and V is affected by $\zeta$, $\xi$ and $l_{KO}$, and is also not constant to zero.

Establish a function for the maximum value of the difference in tendon rope changes during wrist rotation,

$$\begin{aligned} F &= \max(f(\gamma)), \gamma \in (0, 45) \\ G &= \max(g(\zeta)), \zeta \in (0, 45) \end{aligned} \quad (10)$$

In which, $F$ is maximum value of difference in the length change of tendon ropes II and III, [mm]; $G$ is maximum value of difference in the length change of tendon ropes IV and V, [mm].

The relationships between $F$ and its parameters and between $G$ and its parameters are shown in Fig. 6 and Fig. 7.

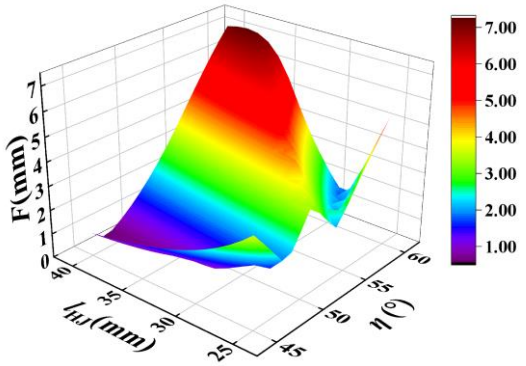


**Fig. 6 – Plot of $F$ against $\eta$ and $l_{HJ}$**

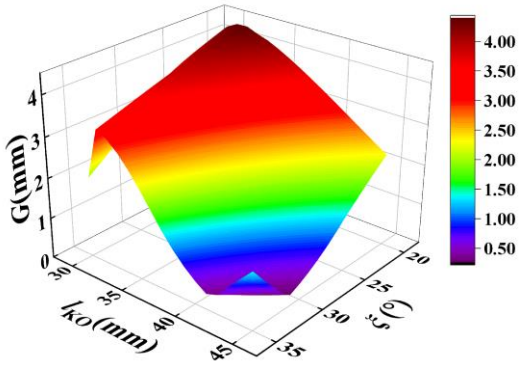


**Fig. 7– Plot of $G$ against $\xi$ and $l_{KO}$**

Use the genetic algorithm toolbox in Matlab to analyze and calculate the configuration parameters of the wrist to meet design requirements. Taking Equation (10) as the objective function, whose value is minimized as the optimization objective, $\eta$, $l_{HJ}$, $\xi$ and $l_{KO}$ are used as the design variables.

The range of values of $(\eta, l_{HJ}, \xi, l_{KO})$ is chosen to be [(45,25,20,30); (60,40,35,45)]. Setting an initial population size of 200, a crossover probability of 0.6, a variance rate of 0.007, a number of iterations of 5000. The outputs are $\eta$ =60, $l_{HJ}$ =25.5, $\xi$ =31.2, $l_{KO}$ =45, $F$ =0.31and $G$ =0.24.

During wrist rotation, although there is a difference in the amount of change in the length of the two tendon ropes, after optimization of the wrist configuration, the difference is minimized to a reasonable range. Constructing a wrist control model based on the amount of tendon rope change on the tightening side, according to Equation (3),(7) yields.

$$\theta_2 = \frac{\sqrt{l_{HI}^{\ 2} + l_{HJ}^{\ 2} - 2\cos(\eta-\gamma) l_{HJ} l_{HI}} - l_{JI}}{r_2} \tag{11}$$

where, $\theta_2$ is the rotation angle of the winding spool II, $r_2$ is the radius of the winding spool II.

$$\theta_1 = \begin{cases} \dfrac{\sqrt{l_{KO}^{\ 2} + l_{KN}^{\ 2} - 2\cos(\kappa-\xi-\zeta) l_{KO} l_{KN}} - l_{ON}}{r_1} & \zeta \le \zeta_0 \\ \dfrac{\sqrt{l_{KO}^{\ 2} + l_{KM}^{\ 2} - 2\cos(\frac{\pi}{2}-\xi-\zeta) l_{KO} l_{KM}} - l_{ON} - l_{NM}}{r_1} & \zeta > \zeta_0 \end{cases} \tag{12}$$

where, $\theta_1$ is the rotation angle of the winding spool I, $r_1$ is the radius of the winding spool I.

Equation (11)(12) construct a model for controlling the rotation angle of the wrist and clarify the relationship between the rotation angle of the wrist and the rotation angle around the spool.

## RESULTS

### *Picking effect experiment*

Produce a physical prototype of the manipulator and conduct field tests in the orchard. Through several picking tests and slow playback observation of the picking process, it is found that the end-effector rotation of 720° can ensure that the fruit stalks are unscrewed, and the time required to complete the picking is 1.6s.

The picking effect of the manipulator was tested under the wrist in the vertical state (Fig. 8) and the deflection state (Fig. 9). The experimental results showed that the success rate of picking by rotating the gripper was 90% under two different wrist states. Due to some fruits being placed between two thicker branches, the gripper was unable to rotate and pick them. The overall success rate was 100%, and no other fruits were detached during the picking process. The test results showed that the success rate of picking by rotating the end-effector under the two wrist states was 90%, which was due to the fact that some of the fruits were in between two thicker branches, which caused the end-effector to be unable to rotate for picking. Picking can be accomplished by pulling and tugging after the end-effector is grasped, with an overall success rate of 100%, and without causing the rest of the fruits to fall off during the picking process.

*a. start* *b.grasp* *c.rotating* *d.complete*

**Fig. 8 – Picking process with wrist in vertical state**

*a. start* *b.grasp* *c.rotating* *d.complete*

**Fig. 9 – Picking process with wrist in deflection state**

The surface of the fruit was intact after picking, and the fruit picked manually was used as a reference to observe the damage of the fruit flesh in the contact area with the manipulator. After 9 days of placement, the fruit flesh in both the finger contact area and the manipulator contact area were intact and free of damage injury, as shown in Fig. 10, indicating that the manipulator was capable of accomplishing non-destructive picking operations.

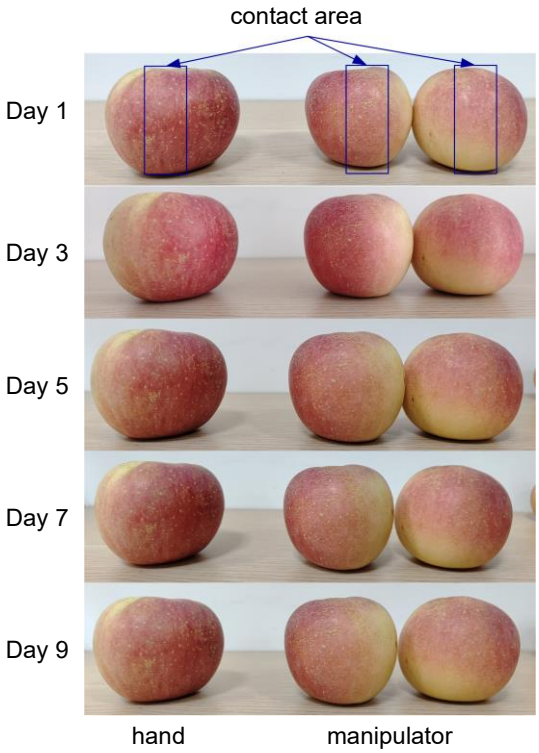


**Fig.10 – Flesh damage test**

## CONCLUSIONS

The rope-driven underactuated picking manipulator designed in this paper has an internally and externally nested double gimbaled wrist structure, and the wrist can be rotated 45° positively or negatively around the x and y axes. The end-effector is able to rotate continuously in a full circle while the wrist rotates, dramatically increasing the flexibility of the manipulator.

Using ANSYS to simulate the performance of different specifications of the hose in different working conditions, the feasibility of the hose as a transmission component is verified, and the PVC hose of 4*6mm (inner diameter*outer diameter) is selected to replace the internal cardan joints to reduce the installation precision requirements and reduce the cost of non-standard parts manufacturing.

With the objective of minimizing the difference in the amount of tendon rope changes between the two sides, the wrist conformation parameters were optimized by genetic algorithm, which reduced the difference in the amount of tendon rope changes to 0.31 mm and 0.24 mm. Through geometric mathematical modeling, the relationship between the winding spool angle and the wrist angle was clarified, and the wrist angle control model was constructed.

The results of the field picking test in the orchard show that the end-effector rotation of 720° can ensure that the fruit stalk is unscrewed, and the time required to complete the picking is 1.6s. The picking operation could be carried out with the wrist in both the vertical and deflected states, with an overall success rate of 100%, and the picking process did not result in the dislodging of the rest of the fruit. The surface of the picked fruit was intact, and the flesh in the area in contact with the manipulator was intact after 9 days of placement, indicating that the manipulator is capable of accomplishing non-destructive picking operations.

## ACKNOWLEDGMENT

This work was funded by the Top Talents Program for One Case One Discussion of Shandong Province, the Key Research and Development Program of Shandong Province (Major Innovative Project in Science and Technology) (2020CXGC010804), Shandong Provincial Natural Science Foundation (ZR2021MC026).

## REFERENCES


[1] Bao G J, Zhang S B, Chen L, et al. (2013). Design of spherical fruit end-grasper based on FPA (基于气动柔性驱动器的球果采摘抓持器). *Transactions of the Chinese Society for Agricultural Machinery*. Vol.44, Issue 05:242-246.

[2] Bu L X, Chen C K, Hu G R, et al. (2020). Technological development of robotic apple harvesters: A review. *INMATEH-Agricultural Engineering*, Vol. 61, Issue 2:151-164.

[3] Bu L X, Chen C K, Hu G R, et al. (2020). Assessment of apple damage caused by a flexible end-effector[J]. *INMATEH-Agricultural Engineering*, Vol. 62, Issue 3:309-319.

[4] Boisclair, J., Laliberté, T., and Gosselin, C., 2022, On the design of an adaptable underactuated hand using rolling contact joints and an articulated palm. *Journal of Mechanisms and Robotics*, Vol. 15, Issue 5:051001.

[5] Chen Q, Yin C K, Guo Z L, et al. (2023). Current status and future development of the key technologies for apple picking robots (苹果采摘机器人关键技术研究现状与发展趋势). *Transactions of the Chinese Society of Agricultural Engineering*, Vol.38, Issue 4: 1-15.

[6] Chen Z W, Yang M J, Li Y W, et al. (2021). Design and experiment of tomato picking end-effector based on non-destructive pneumatic clamping control(基于气动无损夹持控制的番茄采摘末端执行器设计与试验). *Transactions of the Chinese Society of Agricultural Engineering*，Vol. 37, Issue 2:27-35.

[7] Deng X L, Luo Z Y, Pang J Q, et al. (2019). Design and experiment of bionic nondestructive handheld suction apple picker(仿生无损吸取式苹果采摘装置的设计与试验). *Journal of China Agricultural University*. Vol. 24, Issue 10:100-108.

[8] Goulart R, Jarvis D, Walsh K B. (2023). Evaluation of end effectors for robotic harvesting of mango fruit. *Sustainability*, Vol. 15, Issue 8:6769.

[9] Hohimer C J, Wang H, Bhusal S, et al. (2019). Design and field evaluation of a robotic apple harvesting system with a 3d-printed soft-robotic end-effector. *American Society of Agricultural and Biological Engineers*, Vol. 62, Issue 2:405–414.

[10] Hua H L, Song J, Zhao J B, et al., (2023), Sensor-Less Grasping Force Control of a Pneumatic Underactuated Robotic Gripper. *Journal of Mechanisms and Robotics*, Vol. 16, Issue 3:031005.

[11] Li T, Qiu Q, Zhao C J, et al. (2021). Task planning of multi-arm harvesting robots for high-density dwarf orchards(矮化密植果园多臂采摘机器人任务规划). *Transactions of the Chinese Society of Agricultural Engineering.* Vol. 37, Issue 2:1-10.

[12] Long Y L, Wang B L, Jin H J, et al. (2023). Variable stiffness actuator and variable stiffness flexible gripper based on differential gear train(基于差动轮系的变刚度执行器及变刚度柔性手爪). *Journal Of Mechanical Engineering*. Vol. 59, Issue 01:91-102.

[13] Stevanović I, Ilić U, Rodić A. (2023). Prototyping of robot harvester for plum farmyards–mechanical design. *Advances in Service and Industrial Robotics,* Vol.135, 470-477.

[14] Vítor T, Manuel F S, Filipe N S, et al. (2023). Design and control architecture of a triple 3 dof scara manipulator for tomato harvesting, *2023 IEEE International Conference on Autonomous Robot Systems and Competitions,* pp. 87-92,

[15] Wei B, He J Y, Shi Y, et al. (2021). Design and Experiment of Underactuated End-effector for Citrus Picking(欠驱动式柑橘采摘末端执行器设计与试验). *Transactions of the Chinese Society for Agricultural Machinery*, Vol. 52, Issue 10:120-128.

[16] Wang X, Kang H, Zhou H, et al. (2023). Development and evaluation of a robust soft robotic gripper for apple harvesting. *Computers and Electronics in Agriculture*, 204: 107552.

[17] Yu F H, Zhou C Q, Yang X, et al. (2022). Design and Experiment of Tomato Picking Robot in Solar Greenhouse[J]. *Transactions of the Chinese Society for Agricultural Machinery*. Vol. 53, Issue 01:41-49.

[18] Zhao Y W, Geng D X, Liu X M, et al. (2019). Kinematics analysis and experiment on pneumatic flexible fruit and vegetable picking manipulator(气动柔性果蔬采摘机械手运动学分析与实验). *Transactions of the Chinese Society for Agricultural Machinery*, Vol. 50, Issue 08:31-42.

[19] Zhi H, Li Z X, Ding X T, et al. (2023). Design and experiment of end effect for kiwifruit harvesting based on optimal picking parameters. *INMATEH-Agricultural Engineering*, Vol. 69, Issue 1:325-334.